

**NASA TECHNICAL
MEMORANDUM**

N 7 1 - 3 6 1 1 3
NASA TM X-67921

NASA TM X-67921

**CASE FILE
COPY**

**MAXIMUM PROPELLANT UTILIZATION IN AN
ELECTRON-BOMBARDMENT THRUSTER**

by Harold R. Kaufman and Allan J. Cohen
Lewis Research Center
Cleveland, Ohio

TECHNICAL PAPER proposed for presentation at
Symposium on Ion Sources and Formation of Ion Beams
Upton, New York, October 19-21, 1971

MAXIMUM PROPELLANT UTILIZATION IN AN ELECTRON-BOMBARDMENT THRUSTER

Harold R. Kaufman and Allan J. Cohen
National Aeronautics and Space Administration
Lewis Research Center
Cleveland, Ohio

Abstract

Current theory and experimental data on propellant utilization in electron-bombardment ion thrusters are reviewed. Because the majority of investigations have been conducted with mercury, the presentation emphasizes that propellant. The results are presented in as general a form as possible to facilitate use in areas other than space propulsion.

Introduction

Electron-bombardment ion sources have been used in ion thrusters since 1960.¹ The need in electric space propulsion is for large ion currents, but with low enough current densities to permit the integration of the source with long-lived accelerators. The typical range of interest for exhaust velocities in ion thrusters is 20 000 to 40 000 m/sec, which is low compared with most physics-experiment ion-beam applications. This exhaust-velocity range of interest results from a mission compromise between high propellant mass at low exhaust velocities and high powerplant mass (usually solar-cell arrays) for high exhaust velocity.

Neutral propellant atoms also escape through the accelerator during normal operation, and are the loss of particular interest in this investigation. Thruster efficiency is defined

$$\eta_t = \frac{F^2}{2\dot{m}P} \quad (1)$$

where (in SI or mks units) F is the thrust in newtons, \dot{m} is the total propellant flow rate in kg/sec, and P is the total thruster input power in watts. In terms of the propellant flow that is ionized and ejected from the thruster, \dot{m}_i , and the propellant utilization η_u ($\eta_u = \dot{m}_i/\dot{m}$), Eq. (1) can be rewritten

$$\eta_t = \frac{\eta_u F^2}{2\dot{m}_i P} \quad (2)$$

The power efficiency is defined

$$\eta_p = \frac{F^2}{2\dot{m}_i P}, \quad (3)$$

so that the thruster efficiency can also be written

$$\eta_t = \eta_u \eta_p. \quad (4)$$

The thruster efficiency is thus proportional to propellant utilization, and an improvement in propellant utilization can be translated directly into improved thruster performance.

The purpose of this paper is to describe the current state of the art for propellant utilization in bombardment-thruster ion sources, to present experimental performance in as generalized and useful a form as possible, and to indicate where future improvements might be expected. Because the majority of experimental and theoretical investigations have been conducted with mercury, the performance will of necessity be slanted toward that propellant. The use of other propellants will also be discussed to assist the reader whose primary interest is other than space propulsion.

Typical Operation

During typical operation with mercury the neutral density corresponds to about 10^{-4} torr, or $\sim 10^{18}$ mercury atoms per m^3 at $\sim 500^\circ$ K ion-chamber wall temperature. The ions are only about 10 percent as dense as the neutrals ($\sim 10^{17}/m^3$) and the electron density equals that of the ions. All of these densities are approximate mean values for the ion chamber as a whole when operated at design conditions. Special locations, such as the vicinity of a hollow cathode could result in large departures from the values given. The ion-chamber electron distribution is usually treated theoretically as a monoenergetic "primary" population superimposed on a low energy Maxwellian background population. The primary electrons actually have, of course, a spread in energy. The use of the monoenergetic approximation, though, greatly reduces the complexity of calculations for a two-group distribution while introducing no substantial errors. Roughly 10 percent of the electrons are energetic primaries at normal operating conditions. The mean energy of these primaries corresponds to about the total potential difference across the discharge. The background Maxwellian population has a temperature of about 5 eV.

The physical cause for a two-group electron distribution resides in the collision probabilities for primary electrons emitted by the cathode. For the typical 30 to 40 eV primary electron, the probability of an ionizing or exciting collision is about 10 times as great as the probability of Coulomb randomization with the low energy background electrons. The high-energy primary population therefore comes from cathode

emission and is decoupled from the low-energy Maxwellian population.

Roughly half of the ions produced within the ion chamber come from primaries, while the rest come from the "tail" of the low-energy Maxwellians.² At high utilization conditions, the fraction of primaries can increase substantially, resulting in most of the ions coming from primaries at these conditions.³

The Debye shielding distance is $\sim 5 \times 10^{-3}$ cm for typical ion-chamber conditions. This small Debye shielding distance, when compared with ion-chamber dimensions, justifies the assumption of equal electron and ion densities. The bulk of the ion-chamber plasma is within a few volts of a uniform potential. The level of this nearly uniform potential is typically ~ 5 V above anode potential. Because of the small Debye shielding distance, sheaths near the anode and cathode are quite thin.

The ion density is normally much less than the neutral density, but far more ions than neutrals leave through the accelerator system. This apparent discrepancy is because of the difference in velocities within the ion chamber for these two species. The neutral velocity is controlled by the wall temperature of $\sim 500^\circ$ K. The ion velocity results from electrostatic fields within the ion-chamber plasma and is the minimum value found necessary by Bohm⁴ for sheath stability at boundaries of ion production regions.

The rapid escape of ions is also involved in the production of multiply charged ions. Multiple ionizations, if significant, are produced by the initial collisions of electrons with neutrals. That is, ionizing collisions of electrons with previously ionized atoms are infrequent and can generally be ignored. Because a variety of charge-to-mass ratios produces a spread in ion beam velocity and a loss in power efficiency, it is customary to operate ion-thruster discharges at voltages such that only a small fraction of multiply charged ions are produced.

The magnetic field strengths employed vary inversely with thruster diameter.⁵ For a 10-cm diam anode, the typical field strength is 1 to 5×10^{-3} T (10 - 50 G). This field strength is sufficient to contain the energetic primary electrons, but has little effect on the ion trajectories.

Electron-bombardment thrusters have been operated on propellants other than mercury. Next to mercury, cesium has been the most used propellant.^{6,7} A much smaller amount of operation has been obtained with gaseous propellants. An early study was made with gaseous propellants in a 10-cm diam thruster.⁸ More recently a study has been made using a divergent-field thruster.⁹ The operation with cesium departs sharply from the preceding description for mercury.

The lower discharge potential differences with cesium (~ 10 V) result in rapid randomization of electrons emitted by the cathode. As a result, a single Maxwellian distribution is found for the electrons instead of the two-group distribution obtained with mercury and most other propellants. The Coulomb randomization of electrons varies inversely as the square of electron energy. The reduced discharge voltage of cesium relative to mercury is therefore the cause of this electron-distribution difference. For discharges over about 20 V (of interest for most propellants) the assumption of the two-group electron distribution should be reasonable.

The temperature of the Maxwellian background electrons is related to the excitation cross section. In mercury the excitation cross section becomes significant near 5 eV. It is not surprising, then, that measured Maxwellian temperatures are typically 5 ± 2 eV. Estimates for Maxwellian temperatures with other propellants should therefore be guided by excitation cross-section knowledge -- if available.

Primary-Electron Region

Recent high-performance ion-chamber designs have used sharply divergent field shapes in which the field strength passes through zero at an axial location near the accelerator and screen grids. Examination of ion-chamber probe surveys^{2,10} have shown that the primary electrons are not found throughout the ion chamber. Instead, the primary electrons are concentrated in a region defined approximately by magnetic-field lines (guiding centers) that do not intercept the anode. In a divergent-field thruster this primary-electron region is located close to the accelerator and screen grids, as indicated by the cross-hatched region in Fig. 1. In this region are the two subregions, one that can be reached directly by electrons emitted by the cathode and one that can be reached only after collisions. The Maxwellian electrons have much less energy than the primary electrons, and thus can be largely reflected by the anode sheath. The Maxwellian electrons are therefore not confined to field lines that do not intercept the anode, and occupy the entire ion-chamber volume.

The overriding importance of the primary-electron region to ion-chamber performance has been shown by the wide range of configuration changes that can be made outside this region with only small effects on performance.³

An early attempt to predict bombardment-thruster utilization assumed uniform conditions throughout the ion chamber.¹¹ Such an approach is clearly not suitable for divergent-field designs. A more recent study of propellant utilization was concerned with conditions in only the primary-electron region.³ The theory presented in this recent study is summarized in the next section.

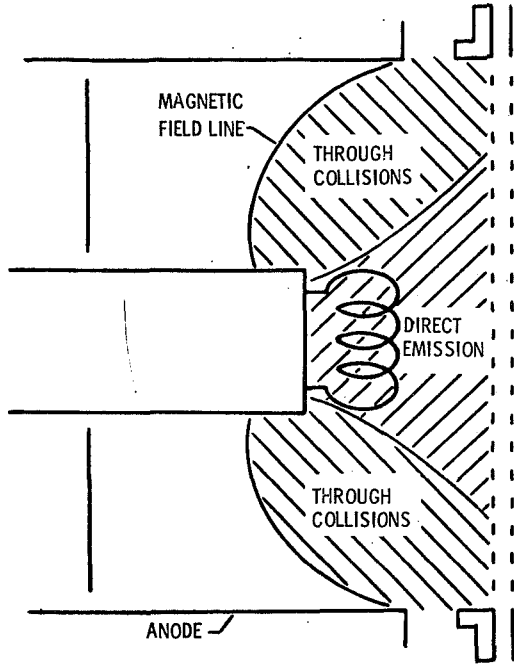


Figure 1 - Primary-electron region (shown by crosshatching) of divergent-field thruster.

Maximum-Utilization Theory

The density of primary electrons increases with discharge current.³ For a maximum-utilization condition at high discharge current, then, ion production should be approximated by considering only primary electrons. Using mean values for the primary-electron region, the total ion production rate \dot{N} from primary electrons is

$$\dot{N} = n_p v_p n_0 \sigma V_p, \quad (5)$$

where n_p and v_p are the primary electron density and velocity, n_0 and σ are the neutral density and ionization cross section, and V_p is the volume of the primary electron region. For the total loss rate of ions from this region,

$$\dot{N} = n_i v_i A_p, \quad (6)$$

where n_i and v_i are the ion density and velocity toward the outer boundary of the primary-electron regions and A_p is the area of that outer boundary. Equating of the loss and production rates followed by solution for neutral density yields

$$n_0 = \frac{(n_i/n_p)(v_i/v_p)}{\sigma(V_p/A_p)}. \quad (7)$$

This equation can be used in a simplified form by assuming a limiting condition where all electrons are primary electrons. Plasma neutrality then requires that $n_i/n_p = 1$. To evaluate v_i/v_p , we use the minimum ion velocity from the Bohm criterion. This minimum ion velocity can be written $v_i = v_p \sqrt{m_e/2m_i}$, where v_p is the mean primary-electron velocity, and m_e and m_i are the electron and ion masses. With these substitutions in Eq. (7),

$$n_0 = \frac{\sqrt{m_e/2m_i}}{\sigma(V_p/A_p)}, \quad (8)$$

All parameters of Eq. (8) are constants, giving a constant value for neutral density n_0 at maximum utilization. (Note that the ratio V_p/A_p is a characteristic length for the primary-electron region, and that this length should vary in a roughly proportional manner with ion-chamber diameter.) A constant neutral density upstream of the accelerator system implies a constant loss of neutrals at maximum propellant utilization regardless of the total mass flow.

A more sophisticated relationship can be obtained by using the previously mentioned combination of monoenergetic primaries and background Maxwellians for the electron distribution. A modified Bohm criterion has been derived by Masek² based on this two-group electron distribution. Using this approach, Eq. (7) becomes

$$n_0 = \frac{\sqrt{m_e/2m_i}}{\sigma(V_p/A_p)} \frac{T_m (1 + n_p/n_m)^{3/2}}{\mathcal{E}_p n_p/n_m}, \quad (9)$$

where T_m and \mathcal{E}_p are the Maxwellian electron temperature and primary electron energies -- both in eV, and n_p/n_m is the primary-to-Maxwellian density ratio.

To compare the results of Eqs. (8) and (9), typical values can be used for the various constants. The mass of a mercury ion can be used for m_i , 5×10^{-20} m² used for σ , and 40 eV and 5 eV used for \mathcal{E}_p and T_m . These values yield

$$n_0 = \frac{2.34 \times 10^{16}}{V_p/A_p} \quad (10)$$

from Eq. (8) and

$$n_0 = \frac{0.827 \times 10^{16}}{V_p/A_p} \frac{(1 + n_p/n_m)^{3/2}}{n_p/n_m} \quad (11)$$

from Eq. (9). Equations (10) and (11) can be multiplied by V_p/A_p . The result of this operation for Eq. (11) is plotted in Fig. 2, while the result for Eq. (10) is indicated on the ordinate of Fig. 2. The value of

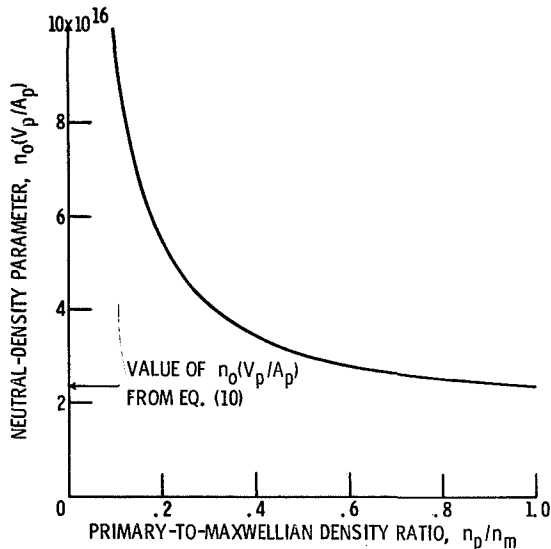


Figure 2. - Variation of neutral-density parameter with primary-to-Maxwellian density ratio from equation (11). Primary energy, 40 eV; Maxwellian temperature, 5 eV.

$n_0(V_p/A_p)$ from Eq. (11) is seen to be higher than the same parameter from Eq. (10) for all values of $n_p/n_m < 1$. Equation (11) is felt to be a more accurate representation of conditions in the primary electron region because of a more accurate electron-distribution representation. On the other hand, Eq. (10) requires less knowledge of ion-chamber conditions, and is therefore easier to use.

Propellant-Utilization Data

Typical ion chamber performance is shown in Fig. 3. The curve for each propellant flow rate is relatively flat below a "knee." Above this knee the curve rapidly becomes nearly vertical. The location of the knee and the nearly vertical portion above the knee depends on propellant flow rate.

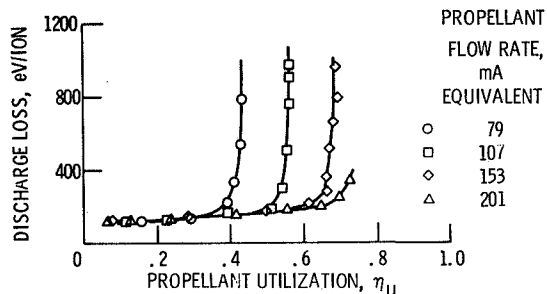


Figure 3. - Typical ion-chamber performance data for a bombardment thruster (from ref. 3).

The investigation that resulted in Eqs. (8) and (9) also compared these equations with experimental ion-chamber data.³ The ion-chamber that was used for these experimental performance data is shown in Fig. 4. (The primary-electron region for this ion chamber was shown in Fig. 1.) Important features of the design were movable and removable parts that permitted different ion-chamber lengths and diameters without affecting the primary-electron region. Also, a refractory metal cathode (tungsten wire) was used to avoid either the evaporation of oxide that can occur at high emission or the propellant concentration that results from the flow through a hollow cathode.

Maximum-utilization data obtained from the ion-chamber of Fig. 4 is shown in Fig. 5. The definition of maximum utilization used for these data was the

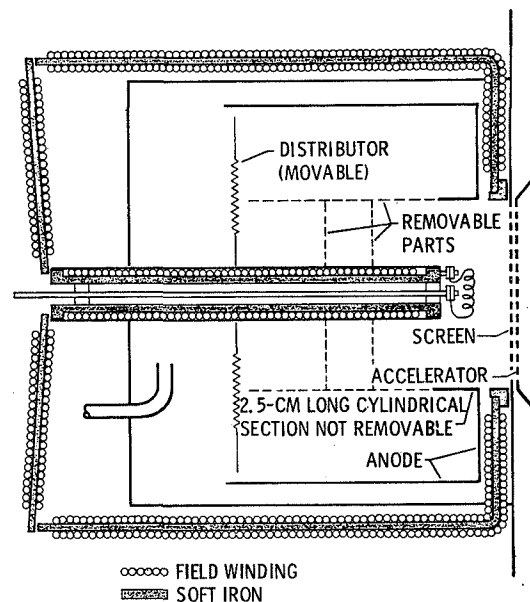


Figure 4. - Ten-centimeter thruster with adjustable ion chamber.

utilization at 1000 eV/ion. This level of discharge loss put the performance well into the near-vertical portion of the ion-chamber performance curves -- as indicated by Fig. 3. The level of neutral propellant loss obtained (Fig. 5(b)) was nearly a constant for a wide range of ion-chamber configurations and propellant flow rates. The level of the neutral loss could be made to agree with both Eqs. (8) and (9) by proper selection of constants. Equation (9) is more complete, and should be more suited to extrapolation to new operating conditions, but it requires knowledge of T_m , ϵ_p , and n_p/n_m that is usually available only from Langmuir probes.

The data of Fig. 5 are quite interesting and instructive in that they show the constant neutral loss

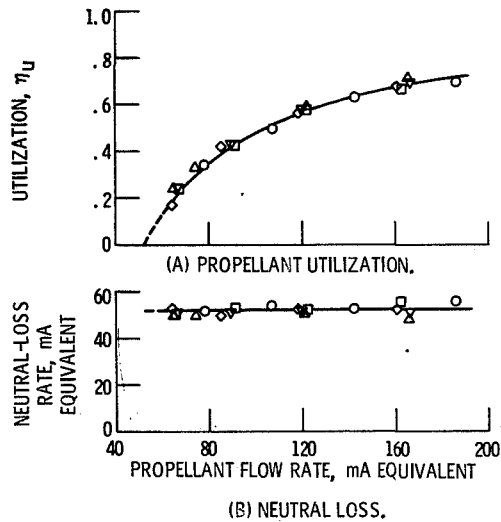


Figure 5. - Correlation of utilization data from 10-cm ion chamber. Discharge loss is 1000 eV/ion. Different symbols indicate different shapes outside primary-electron region.

predicted by Eqs. (8) and (9). Practical applications, though, center around the "knee" of the discharge-loss curve (Fig. 3). If one operates an ion chamber at a utilization below that of the knee, then the propellant flow rate could be reduced with only a small increase in discharge loss. Conversely, if one is operating at some high-discharge loss above the knee, then the discharge loss could be reduced with only a small decrease in utilization.

Accordingly, available ion thruster data were examined with a view toward finding data obtained: (1) near the discharge-loss knee, (2) under good enough experimental conditions (particularly facility size) to assure accurate propellant utilization measurements, (3) over a wide range of propellant flow rate, and (4) with strongly divergent magnetic-field designs. In addition to the 10-cm ion-chamber design shown in Figs. 1 and 4, data were used from chambers with 5-cm, 15-cm, and 30-cm diameters. All three of these ion-chamber designs were the result of much experimental optimization, and all used hollow cathodes. The primary-electron regions and general ion-chamber shapes for these three thrusters are shown in Fig. 6. All of these ion chambers (including the one shown in Fig. 4) were used with about 50-percent open accelerator grids and 65- to 70-percent open screen grids. The effective sharp-edged orifice area for all of these accelerator systems was estimated at one-quarter of the beam area. More detailed descriptions of the 5-cm, 15-cm, and 30-cm thrusters can be found in another paper presented at this conference.¹²

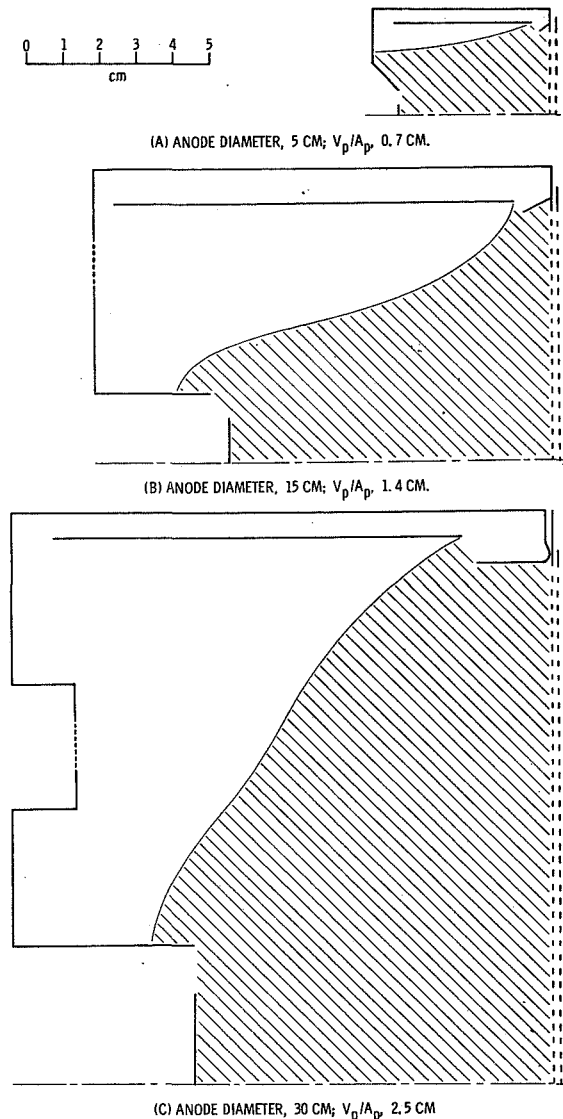


Figure 6. - Primary-electron regions (shown by crosshatching) of current divergent-field bombardment thrusters.

Data obtained near the knee of the performance curves are shown in Fig. 7 for the four ion chambers.¹³⁻¹⁶ With the exception of the 5-cm data, all data were obtained with discharge losses of 250-300 eV/ion. The 5-cm data were obtained at 570 eV/ion. The 5-cm design represents a compromise toward improving the low utilization associated with small size at the expense of a higher discharge loss. This compromise is evident in the deeper (in terms of length-to-diameter ratio) primary-electron region of the 5-cm design shown in Fig. 6. With this deeper region the value of V_p/A_p is increased, but at the expense of a larger fraction of ions produced going to the ion-chamber walls instead of being accelerated into the beam.

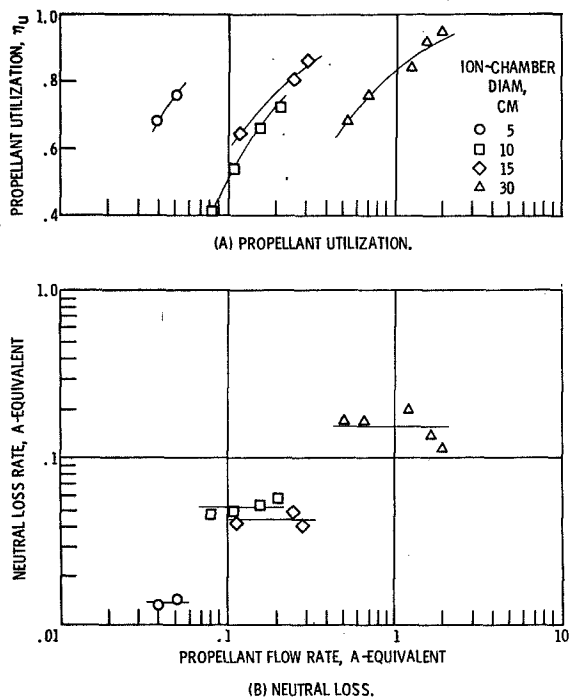


Figure 7. - Utilization data for the "knee" of the discharge-loss curve. Mercury propellant.

The utilization efficiency (Fig. 7(a)) clearly decreases with total propellant flow rate for each of the ion chambers. The corresponding loss in neutrals is shown in Fig. 7(b). The neutral loss wanders over a small range for each thruster, sometimes increasing and sometimes decreasing with increasing total propellant flow rate. In going from the 1000 eV/ion data of Fig. 5 to the "knee" data of Fig. 7, the increase in practical interest has clearly been accompanied by an increase in scatter for each thruster. The data of Fig. 7, though, still indicate that neutral loss is approximately constant for the "knee" data.

A suitable parameter was desired to facilitate comparison of operation with different propellants. Equation (9) would have been used, but it requires more information than is generally available. Instead, Eq. (8) was selected to be the basis for deriving this parameter. The neutral density of Eq. (8) can be expressed as a neutral propellant loss rate \dot{N}_0 when combined with an effective sharp-edged orifice area A_0 for the accelerator system and the average magnitude of neutral velocity \bar{v}_0 ($\bar{v}_0 = \sqrt{8 kT/\pi m}$).

$$\dot{N}_0 = n_0 \bar{v}_0 A_0 / 4 \quad (12)$$

The wall temperature should be roughly the same for all ion chambers. We should therefore be able to write

$$\dot{N}_0 = K n_0 A_0 / m_i^{1/2} \quad (13)$$

where K includes all constants that are not a function of the ion source configuration or the propellant. With the substitution of Eq. (8) for n_0 , Eq. (13) becomes

$$\dot{N}_0 = \frac{K A_0 \sqrt{m_e / 2 m_i}}{m_i^{1/2} \sigma (V_p / A_p)} \quad (14)$$

(Note that for all practical purposes $m_0 = m_i$.) Finally, by redefinition of K ,

$$\dot{N}_0 = K A_0 / m_i \sigma (V_p / A_p) \quad (15)$$

When solved for K ,

$$K = \dot{N}_0 m_i \sigma (V_p / A_p) / A_0 \quad (16)$$

Thus the product $\dot{N}_0 m_i \sigma (V_p / A_p) / A_0$ should be nearly constant for all ion chambers.

The data of Fig. 7 were replotted in Fig. 8 in terms of the neutral loss parameter $\dot{N}_0 m_i \sigma (V_p / A_p) / A_0$. For convenience, the neutral loss rate \dot{N}_0 was expressed as equivalent amperes (the current that would be measured if each atom had one electronic charge), and m_i was expressed in atomic mass units. The remaining parameters σ , (V_p / A_p) , and A_0 were expressed in m^2 , m , and m^2 .

In addition to the mercury propellant data of Fig. 7, other gas data are plotted for the 15-cm ion chamber.⁹ Xenon and krypton were used in an unmodified 15-cm thruster, with knee data again obtained in the 250 - 300 eV/ion range. A modified 15-cm ion chamber was used with argon. This modification was to block screen holes except for the center 7.5-cm diameter of the accelerator system. Inasmuch as this modification also blocked much of the ion extraction, the discharge loss was increased to about 750 eV/ion. Values used for the ionization cross section in the neutral-loss parameter were $5 \times 10^{-20} m^2$ for mercury, $5 \times 10^{-20} m^2$ for xenon, $4.5 \times 10^{-20} m^2$ for krypton, and $3 \times 10^{-20} m^2$ for argon. These values were selected to be near the maxima, but still at low enough electron energies that double ionization would be negligible.¹⁷ These gas propellant data were included in Fig. 8.

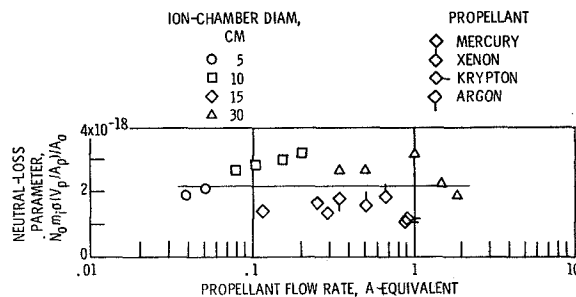


Figure 8. - Neutral-loss parameter for the "knee" of the discharge-loss curve.

Because the mercury data used corresponded to considerable thruster optimization, other gas propellant data were selected for good propellant distribution, near-optimum magnetic-field strength, and a moderate discharge voltage (to minimize multiple ionization). Further, no data were used for propellants that required much higher discharge losses (neon and helium), because it was felt that the higher losses were indicative of some other than normal mode of operation. (It appeared that the neutral flow required for the hollow cathode to operate with neon and helium was too much for good ion-chamber performance. This viewpoint is supported by the fact that the earlier gas-thruster investigation actually gave better performance with these gases.⁸)

One can conclude from Fig. 8 that for the range of propellant flow rates investigated, the range of propellants used, and a strongly divergent magnetic-field design, the neutral loss parameter is about $2.1 \pm 1.1 \times 10^{-18}$. The degree of correlation appears good enough to permit use of this parameter as an approximate design tool. Because the data of Fig. 8 were obtained with at least some selection of operating conditions and/or optimization, the use of the neutral-loss parameter should be considered as merely an adjunct to good design.

Earlier bombardment ion-source data using gaseous propellants and only a moderate degree of magnetic-field divergence⁸ were not included in Fig. 8. The magnetic field at the middle of the accelerator was about 80 percent of the maximum value in the chamber for this earlier data, while the field strength drops to nearly zero at the same location in strongly divergent designs. Some checks were made of this earlier data. The neutral-loss parameters were found to be two to three times as large as for strongly divergent designs.

Concluding Remarks

The primary-electron region plays an important role in the ionization processes of a bombardment-thruster ion chamber. From both analyses of the primary-electron region and experimental data, neutral propellant losses have been shown to be nearly constant at high discharge-loss conditions -- regardless of total propellant flow rate.

A region of more practical interest is the knee of the discharge loss curve, which generally represents the best compromise between discharge losses and neutral propellant losses. The neutral losses at the knee of the performance curve are not as constant for a given thruster as at the high discharge loss condition. But the neutral losses are still near enough constant to use for an estimate of utilization over a range of total propellant flow rate.

A neutral-loss parameter was obtained. This parameter was experimentally evaluated for several

different propellants and ion-chamber sizes that have been used with strongly divergent magnetic-field designs. The correlation indicates that this neutral-loss parameter may be useful as a design tool.

Future improvements in performance of bombardment ion thrusters could come in part from proper shaping of the primary-electron region. A roughly hemispherical shape would appear near optimum; that is, optimum from the viewpoint of maximizing the ratio V_p/A_p without excessively increasing A_p , as well as providing a fairly flat ion-beam profile.

The shape of the primary-electron region shown in Fig. 1 would therefore appear desirable. Unfortunately, the field lines within this region result in a peaked ion-beam profile when the magnetic field is increased to minimize discharge losses. What is really needed, then, is a roughly hemispherical shape with near zero magnetic-field strength inside the primary-electron region and a strong magnetic field outside. Although these requirements may sound mutually exclusive, there is a magnetic-field design that may come close to satisfying them. This design is the multipole "picket fence" concept of plasma containment from fusion research. The multipole design has been used in a cesium thruster with high performance,⁹ but the results with mercury have been mixed.^{18,19} Some development of the multipole design appears likely for future high-performance bombardment thrusters.

References

1. H. R. Kaufman and P. D. Reader, "Experimental Performance of Ion Rockets Employing Electron-Bombardment Ion Sources," ARS Paper 1374-60 (1960).
2. T. D. Masek, "Plasma Characteristics of the Electron Bombardment Ion Engine," Jet Propulsion Lab., Calif. Inst. Tech. TR-32-1271 (1968).
3. H. R. Kaufman, "Ion-Thruster Propellant Utilization," Colorado State University, Ph.D. Thesis (1971).
4. D. Bohm, The Characteristics of Electrical Discharges in Magnetic Fields, A. Guthrie and R. K. Wakerling, eds., (McGraw-Hill, New York, 1949), pp. 77-86.
5. P. D. Reader, ARS J. 32, 711 (1962).
6. R. C. Speiser and L. K. Branson, "Studies of a Gas Discharge Cesium Ion Source," ARS Paper 2664-62 (1962).
7. R. D. Moore, S. Goldner, R. C. Speiser, and R. Vernon, "Cesium Electron Bombardment Thruster Research," Electro-Optical Systems, Inc. Rep. EOS-7240-Final, NASA CR-98913 (1968).

8. P. D. Reader, "The Operation of an Electron-Bombardment Ion Source with Various Gases," NASA TM X-52006 (1964).
9. D. C. Byers and P. D. Reader, "Operation of an Electron-Bombardment Ion Source Using Various Gases, Proposed NASA Tech. Note (1971).
10. W. Knauer, R. L. Poeschel, H. J. King, and J. W. Ward, "Discharge Chamber Studies for Mercury Bombardment Ion Thrusters," Hughes Research Labs., NASA CR-72440 (1968).
11. H. R. Kaufman, "Performance Correlation for Electron-Bombardment Ion Sources," NASA TN D-3041 (1965).
12. W. R. Kerslake and P. D. Reader, "Kaufman Ion Thruster Development at the Lewis Research Center," Paper to be presented at Symposium on Ion Sources (1971).
13. W. C. Lathem, Private communication of 5-cm bombardment thruster data.
14. Reference 3, Figure 12(i) for optimum 10-cm bombardment thruster data.
15. D. C. Byers and J. F. Staggs, *J. Spacecraft Rockets* 7, 7 (1970). (From private communication with Byers, fig. 6(b) in this reference is incorrect. The utilization at 250 eV/ion and a beam current of 0.20 A was close to 0.80.)
16. H. J. King, et al., Proposed NASA Contr. Rep., NASA Contract NAS3-14140, 1971.
17. S. C. Brown, Basic Data of Plasma Physics, 1966, Second Ed., Rev. (M.I.T. Press, Cambridge, 1967).
18. R. L. Poeschel, J. W. Ward, and W. Knauer, *J. Spacecraft Rockets* 7, 26 (1970).
19. W. Ramsey, "12 Centimeter Magneto-Electrostatic Containment Mercury Ion Thruster Development," AIAA Paper 71-692 (1971).